of electrode/electrolyte/current-collector. The beginning of the semicircle line (left-intercept of Z'' at the Z' axis) represents the resistance (R_s) of the electrolyte in contact with the current collector and electrode. The termination of the semicircle line (right-intercept of Z'' at the Z' axis) represents the internal resistance (R_p) of the electrode. The diameter of the semicircle (R_p-R_s) is equal to the ESR value. The values of R_s, R_p and ESR for all the cells determined from the data in Figure 4 are listed in Table 4. These results do not show any specific trend with respect to changing the carbonization temperature, but the magnitude of the ESR values are typical for carbon based supercapacitors. For example, Kim et al. (2006) have reported the ESR values of 0.134 to 1.149 Ω for the bamboo based activated carbon electrodes [20].

The second segment (straight line with a slope of approximately 45°) in the middle frequency region represents the combination of resistive and capacitive behaviors of the ions penetrating into the electrode pores. The length, slope and position of this segment appear to be affected by changes in the carbonization temperature. A steep slope corresponding to electrodes that efficiently allow ions to penetrate pores has been observed in another study on carbon electrodes from porous carbon powder [31].

The third segment (straight lines sharply increasing at the low-frequency region) represents the dominance of capacitive behavior from the formation of ionic and electronic charges of the electric double layer system at the micropore surfaces; at this frequency, the ions can more easily diffuse into the micropores [31-34]. The initiation point of this third segment line corresponds to the knee frequency (f_k), and its corresponding resistance (R_k) is given by Z'_k. The values of f_k and R_k are given in Table 4. These results seem to show that carbonization at 800°C may change the capacitive region to begin at a relatively higher frequency value with a lower resistance. The length of this straight line is shorter for the ACM8 cell compared to the other two cells; furthermore, the line for the ACM8 cell leans more towards the vertical Z'' axis, indicating that the ACM8 cell has a better capacitive performance. The values of the C_{sp} calculated from the EIS data using equation (1) are shown in Table 5 and reveal that this ACM8 cell has the highest C_{sp}.

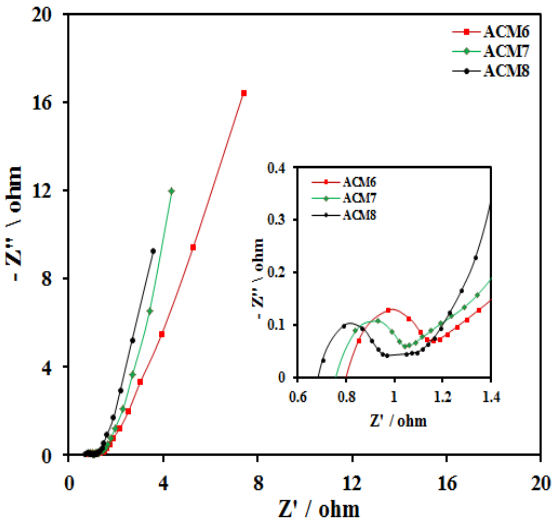

Figure 4. Nyquist plots for the ACM cells.

Table 4. The values of R_s, R_p, ESR, f_k and R_k for the ACM cells.

Cells	R_s (Ohm)	R_p (Ohm)	ESR (Ohm)	f_k (Hz)	R_k (Ohm)
ACM6	0.877	1.084	0.207	5	1.522
ACM7	0.749	1.064	0.315	10	1.344
ACM8	0.860	1.063	0.203	40	1.138

Figures 5 (a) and (b) show the specific, imaginary (*C''*) and real (*C'*) capacitance portions of the ACM cells calculated using equations (1), (3) and (4) as a function of frequency. In Figure 5 (a), the C_{sp} strongly depends on the frequency below 1 Hz, particularly for the ACM8 cell, which shows a higher C_{sp} throughout the entire frequency region. A similar frequency dependency is also exhibited by the *C'* and *C''* curves in Figure 5 (b). For the *C''* curve, there is a peak frequency value (f_p). This frequency value is associated with the relaxation time constant, τ_o, which defines the boundary between the regions of capacitive and resistive behaviors for the supercapacitor. It is well known that higher power delivery corresponds to lower τ_o values.

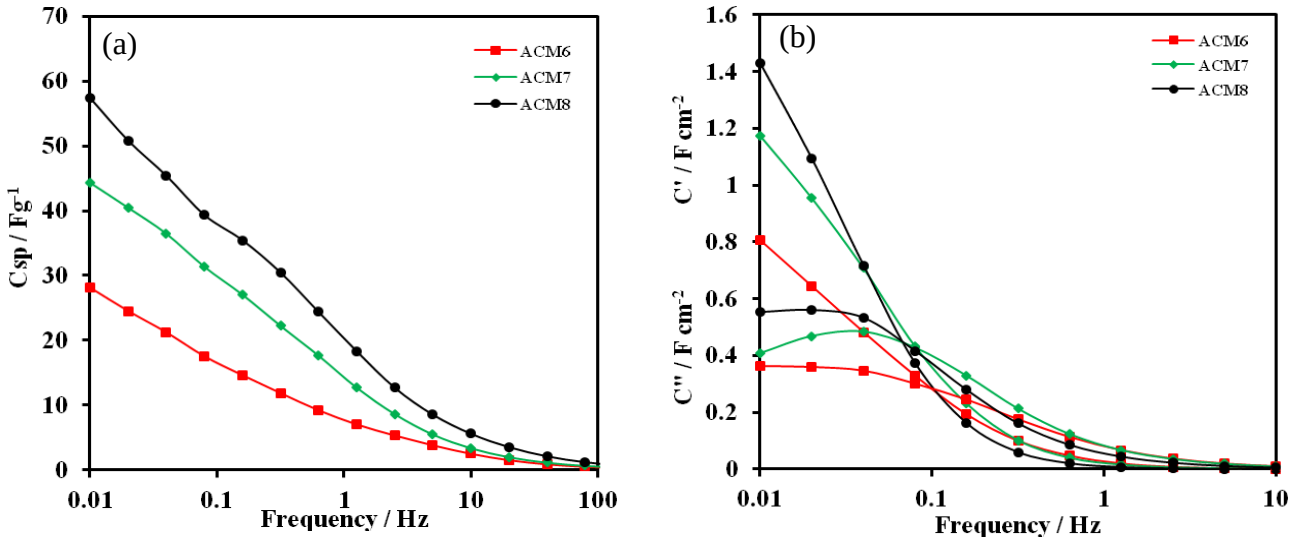

Figure 5. (a) Specific capacitance versus frequency, (b) Evolution of imaginary and real portions of capacitance for the ACM cells.

Based on the f_p values in Figure 5 (b), the value of τ_o was estimated using the equation $\tau_o = 1/f_p$, the results of which are 25.12 and 50.13 s for the ACM7 and ACM8 cells, respectively. The τ_o value for the ACM6 cell cannot be calculated because the peak lies below the detection limit of the instrument. These calculated τ_o values are within the same order of magnitude as that reported by Garcia-Gomes et al. (2010); 3.8 to 62 s for the CM electrodes based on another type of precursor [35].

Other investigations showed values of τ_o in the range of 3 to 68 s for carbon electrodes prepared from micro/mesoporous carbon C(Mo_2C) [36].

3.2.2 Cyclic voltammetry

The supercapacitive properties of the ACM6, ACM7 and ACM8 cells were determined using cyclic voltammetry because this method provides valuable information on the charge-discharge behavior of the cells. The measurements were performed at room temperature within the potential range of 0 to 1 V and over a scan rate of 1 to 100 mVs^{-1}. Fig 6 (a) shows the measured cyclic voltammograms recorded at 1 mVs^{-1} for the ACM6, ACM7 and ACM8 cells. The shape of the voltammograms for all the cells is rectangular, representing a typical voltammogram for electric double-layer capacitance [37]. Comparing the voltammograms of the ACM6, ACM7 and ACM8 cells in Figure 6 (a), it can be observed that the ACM8 cell has a broader voltammogram area. These results indicate that the ACM8 cell has a better cycle reversibility and higher electric double-layer capacitance stability during the charge and discharge processes compared with the other cells. Ultimately, these effects correspond to a higher C_{sp} for the ACM8 cell. The C_{sp} of the ACM6, ACM7, and ACM8 electrodes were calculated using the equation (5) from the voltammograms (Figure 6) recorded with a scan rate of 1 mVs^{-1}. These results are shown in Table 5 and are in good agreement with the obtained EIS results.

It is also observed that the voltammograms (scan rate of 1 mVs^{-1}) in Figure 6 (a) do not have any peaks, which indicates that the supercapacitive behavior is free from redox reactions or is purely based on the electrostatic mechanism. It was also found that this behavior was exhibited by all of the cells when the scan rate was varied up to 100 mVs^{-1}. To observe such a supercapacitive behavior over a range of scan rate, Figure 6 (b) shows the voltammograms for the ACM8 cell at five different scan rates (1, 5, 25, 50, and 100 mVs^{-1}). Figure 6 (b) demonstrates that the current response increased with the scan rate. Furthermore, as the scan rate increased above 5 mVs^{-1}, the voltammograms 'window' tended to tilt toward the vertical axis, thereby becoming a quasi-rectangle. This result indicates the dominance of the double layer formation in the energy storage process at lower scan rates.

Figure 6 (c) shows the C_{sp} values determined using equation (5) and the voltammograms obtained at different scan rates for all the ACM cells. All cells show a common trend of decreasing C_{sp} values against an increasing scan rate. It is well known that for very low scan rates, the C_{sp} values are higher because the ions have a much longer time to penetrate and reside in all the available electrode pores and form electric double layers, which are needed to generate higher capacitance. Despite this common trend, the ACM8 cell displays higher C_{sp} values throughout the whole scan region, clearly indicating its superiority over the other two cells. This result is in agreement with the EIS results discussed in the preceding section. In the scan rate region above 5 mVs^{-1}, the C_{sp} for the ACM8 seemed to decrease faster than that for the ACM6 and ACM7 cells as the scan rate increased; these results are evidence of the increasing diffusion resistance towards the ionic motion into the electrode pores, which is not linear with respect to the change in the carbonization temperature during electrode preparation. This non-linear effect has also been observed in investigations assessing the dependence of electrode C_{sp} on the quantity of binder used during electrode preparation [38].

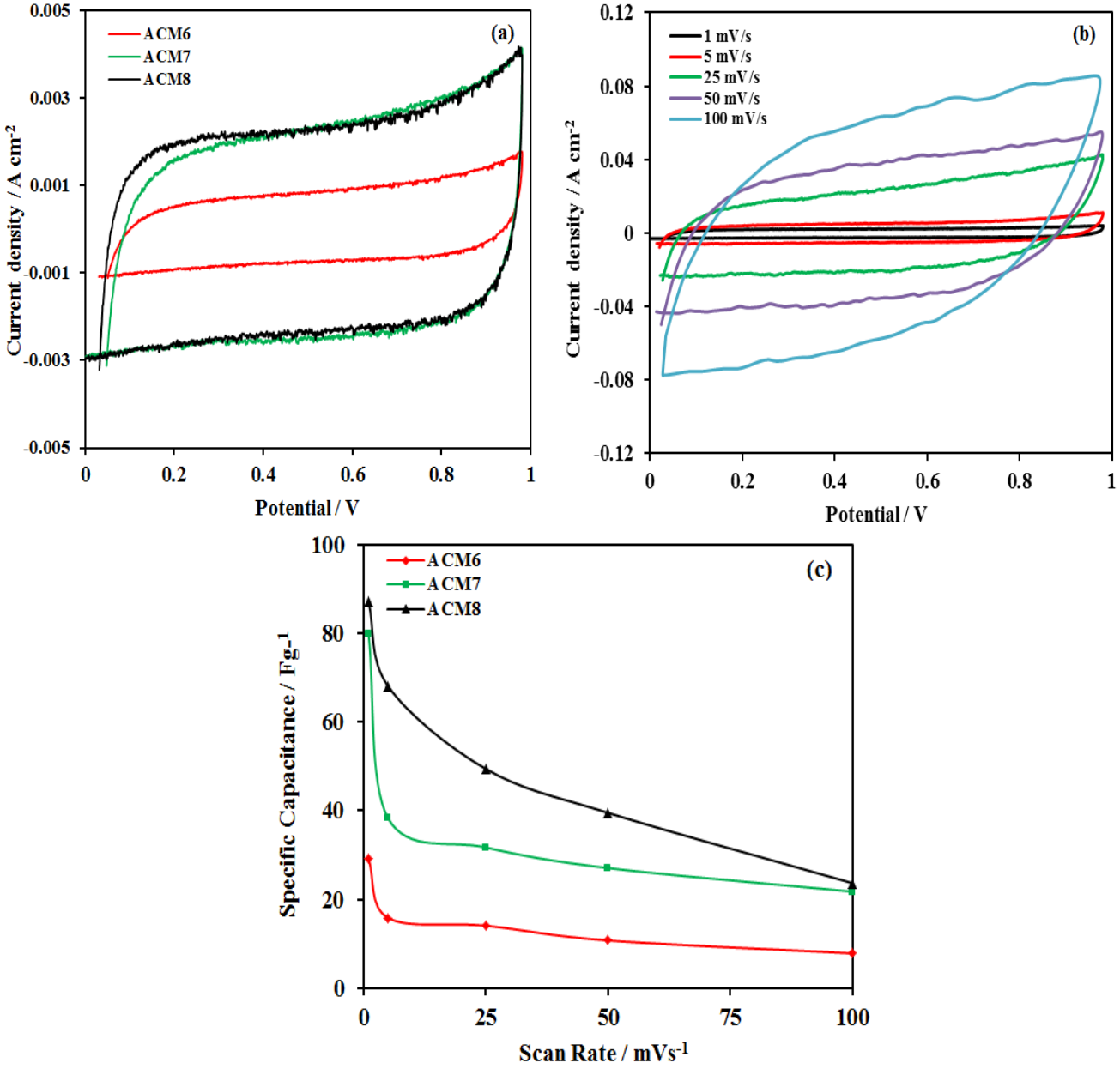

Figure 6. (a) CV curves at the scan rate 1 mVs^{-1} for the ACM cells, (b) CV curves with various scan rates for the ACM8 cell, and (c) Specific capacitance versus scan rate for the ACM cells.

3.2.3 Galvanostatic charge-discharge

The GCD curves for all the ACM cells recorded in the potential range of 0 – 1 V and at a current density of 10 mA cm^{-2} are shown in Figure 7. As seen in this figure, all the cells show a similar symmetrical triangular curve with a nearly linear variation of voltage as a function of time during charge and discharge. This type of curve is typical for carbon-based supercapacitors, and the data shows that all the three cells have a good supercapacitive performance. However, despite having a

similar shape, the curves for the ACM7 and ACM8 cells, particularly the latter, show significantly higher charge and discharge times, as shown in Figure 7; these observations indicate that a higher number of electrons and electrolyte ions are participating in the charge and discharge processes of these electrodes compared to the ACM6 electrode. This is further evidence supporting the results obtained by the EIS and CV methods that determined carbonization temperatures closer or equal to the activation temperature can produce better electrodes for supercapacitor application. Put more directly, the carbonization temperature of 600°C is too low to be compatible with the 800°C activation temperature used during electrode preparation.

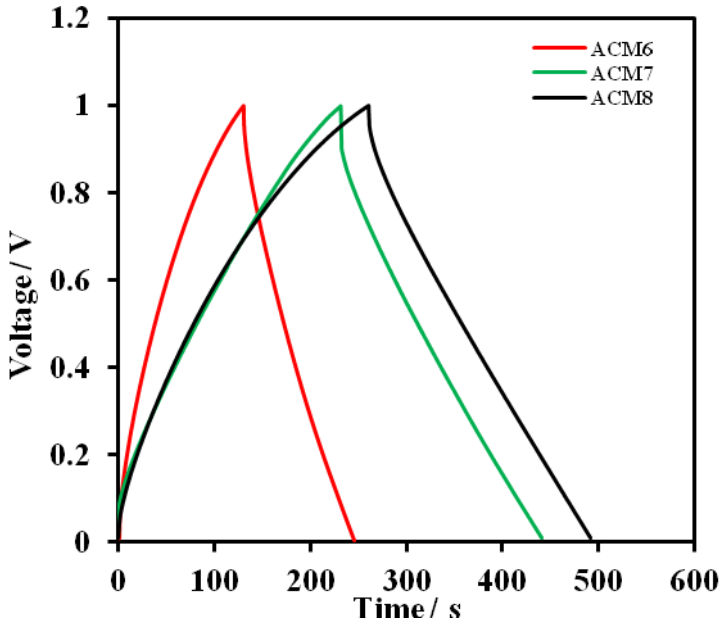

Figure 7. GCD curves for the ACM cells.

As revealed in Figure 7, a sharp drop in the initial voltage upon discharge is evident and results from diffusion-limited mobility of the electrolyte ions in the electrode pores. This limitation is associated with the equivalent series resistance (ESR) of the supercapacitor cells. The ESR value is calculated from this voltage drop using the equation ESR = $iR_{drop}/2i$. The ESR values for the ACM6, ACM7 and ACM8 cells are 2.615, 4.852 and 2.437 Ohm, respectively, clearly indicating that the ACM8 cell offers the lowest ESR value. These ESR values are comparable with the results of other researchers who observed ESR values ranging from 1.17 to 3.69 Ohm for carbon electrode mixtures composed of activated carbon, graphite and polytetrafluoroethylene (PTFE) [39] and from 9.7 to 16.7 Ohm for carbon electrodes derived from activated carbon powder [40]. These literature ESR values derived from the GCD data are higher than those derived from the EIS data. This trend is also observed in the ESR results reported here.

The C_{sp} values of the supercapacitor cells based on ACM electrodes were calculated from the data in Figure 7 using equation (6) and are shown in Table 5. As expected, these values follow the trend of C_{sp} values calculated from the EIS and CV data, i.e., showing a good trend of overall change

in magnitude with respect to the change in carbonization temperature. For comparison, some of the C_{sp} values reported in the literature for other types of carbon electrodes used in supercapacitors are also included in Table 5.

Table 5. Specific capacitance (C_{sp}) for the ACMs cells (x = EIS, y = GCD, z = CV).

Cells	${}^{x}C_{sp}$ (Fg^{-1})	${}^{y}C_{sp}$ (Fg^{-1})	${}^{z}C_{sp}$ (Fg^{-1})
ACM6	28	55	27
ACM7	44	77	78
ACM8	61	85	80
Ref. [2]	-	235-319	226-339
Ref. [8]	38-90	2-176	-
Ref. [9]	-	-	244-311
Ref. [28]	-	135-329	228-358
Ref. [29]	-	230-300	-

3.2.4 Specific energy and power

The specific power and specific energy of the ACM cells were calculated from the GCD curves (Figure 7) using equations (7) and (8), respectively [41]. The results are shown as Ragone plots in Figure 8, which indicate there is a correlation between the specific power and specific energy of the supercapacitor.

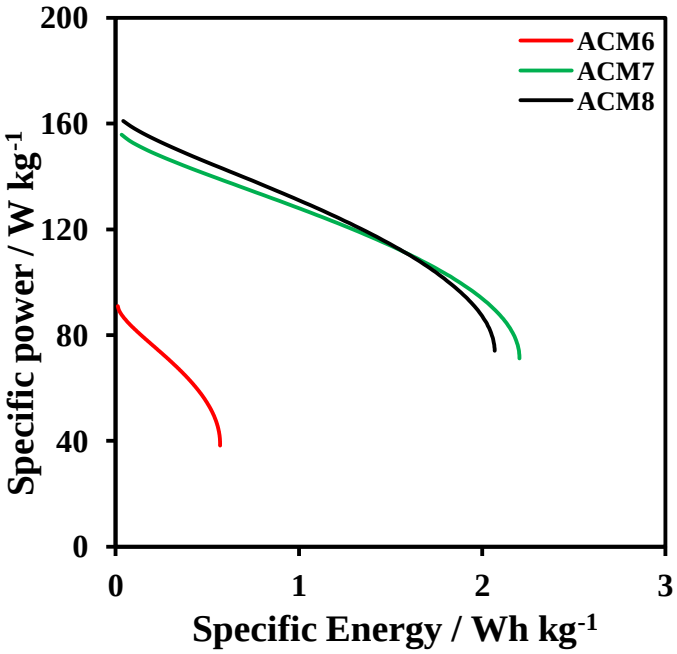

Figure 8. Ragone plots for the ACM cells.

The specific power linearly decreases with increasing specific energy for all the cells, which means that less energy is released at higher power output. However, as shown in Figure 8, the power-energy relationship for the ACM7 and ACM8 cells seem to be much better than that of the ACM6 cell; again demonstrating that the carbonization temperature closer or equal to the activation temperature may help producing better performance of the ACM electrodes for supercapacitor application (also shown by the EIS and CV data in the preceding sections). The maximum specific energy and specific power determined were 2.2 Wh kg^{-1} and 156 W kg^{-1}, respectively, for the ACM7 cells and 2.1 Wh kg^{-1} and 161 W kg^{-1}, respectively, for the ACM8 cells. These results are comparable to the typical ranges of specific energy and specific power values for supercapacitor electrodes derived from other types of biomass precursors, i.e., cherry stones fell within the range of 3.5 to 5 Wh kg^{-1} and 700 to 1900 W kg^{-1}, respectively [29]. A similar range of specific energy and specific power values was observed between 2.6 to 3.3 Wh kg^{-1} and 580 to 620 W kg^{-1}, respectively, for carbon electrodes prepared from rubberwood sawdust precursor [29] and between 0.5 to 3.5 Wh kg^{-1} and 150 to 160 W kg^{-1}, respectively, for carbon electrodes from oil palm empty fruit bunch fibers precursor [11].

4. CONCLUSION

GMs consisting of SACG EFB fibers (95% by weight), CNTs (5%) and KOH (5%) were heated to 600, 700 and 800°C carbonization temperatures (CTs), respectively, to produce CM6, CM7 and CM8. These CMs were activated by CO_2 at 800°C to produce ACM6, ACM7 and ACM8, which were used as electrodes in supercapacitor cells. We observed that the changes in the density, electrical conductivity, porosity, microstructure and structure of the ACMs due to the change in the CT notably affected the electrochemical behaviors of the supercapacitor cells. Characterization by EIS, CV and GCD methods consistently found that the cells using the ACMs from the CMs (CT = 700, 800°C) exhibit better specific capacitance, specific energy and specific power than that from the CM (CT = 600°C). These results lead to the conclusive recommendation that the CT value should be closer or equal to the activation temperature for the production of higher quality ACM electrodes from CMs.

ACKNOWLEDGMENTS

We acknowledge grants from the Universiti Kebangsaan Malaysia (UKM-GUP-216-2011, UKM-DLP-2012-022, and UKM-DLP-2012-023), and the support of CRIM (Centre for Research and Innovation Management). The authors also thank Mr. Saini Sain for helping with the laboratory work.

References

1. Y. Liu, Z. Hu, K. Xu, X. Zheng and Q. Gao, *Acta Phys. Chim. Sin.*, 24(7) (2008) 1143.
2. B. Xu, Y. Chen, G. Wei, G. Cao, H. Zhang and Y. Yang, *Mater. Chem. Phys.*, 124 (2010) 504.
3. P.L. Taberna, G.C. Chevallier, P. Simon, D. Plee and T. Aubert, *Mater. Res. Bull.*, 41 (2006) 478.

4. Q.Y. Li, Z.S. Li, L. Lin, X.Y. Wang, Y.F. Wang, C.H. Zhang and H.Q. Wang, *Chem. Eng. J*., 156 (2010) 500.
5. J.M. Ko and K.M. Kim, *Mater. Chem. Phys*., 114 (2009) 837.
6. L. Chunlan, X. Shaoping, G. Yixiong, L. Shuqin and L. Changhou, *Carbon*, 43 (2005) 2295.
7. C. Grini, *Bioresour. Technol*., 97 (2006) 1061.
8. J.M. Valente Nabais, J.G. Teixeira and I. Almeida, *Bioresour. Technol*., 102 (2011) 2781.
9. X. Li, W. Xing, S. Zhuo, J. Zhou, F. Li, SZ. Qiao and G.Q. Lu, *Bioresour. Technol*., 102 (2011) 1118.
10. Awitdrus, M. Deraman, I.A. Talib, R. Farma, R. Omar, M.M. Ishak, N.H. Basri and B.N.M. Dolah, *Adv. Mater. Res*., 501 (2012) 13.
11. R. Farma, M. Deraman, R. Omar, Awitdrus, M.M. Ishak, E. Taer and I.A. Talib, *AIP Proceeding*, 1415 (2011) 180.
12. M. Deraman, M.M. Ishak, R. Farma, Awitdrus, E. Taer, I.A. Talib and R. Omar, *AIP Proceeding*, 1415 (2011) 175.
13. M. Deraman, R. Omar, S. Zakaria, I.R. Mustapa, M. Talib, N. Alias and R. Jaafar, *J. Mater. Sci*., 37 (2002) 3329.
14. C. Portet, O.L. Taberna, P. Simon, E. Flahaut and C. Laberty Robert, *Electrochim. Acta*, 50 (2005) 4174.
15. M. Beidaghi, W. Chen and C. Wang, *J. Power Sources*, 196 (2011) 2403.
16. K.C. Tsay, L. Zhang and J. Zhang, *Electrochim. Acta*, 60 (2012) 428.
17. A.B. Fuertes, G. Lota, T.A. Centeno and E. Frackowiak, *Electrochim. Acta*, 50 (2005) 2799.
18. S.R.S. Prabaharan, R.Vimala and Z. Zainal, *J. Power Sources*, 161 (2006) 730.
19. M. Deraman, S. Zakaria, R. Omar and A.A. Aziz, *Jpn. J. Appl. Phys*., 39 (2000) L1236.
20. Y.J. Kim, B-J Lee, H. Suezaki, T. Chino, Y. Abe, T. Yanagiura, K.C. Park, M. Endo, *Carbon*, 44 (2006) 1592.
21. E. Taer. M. Deraman, I.A. Talib, A.A. Umar, M. Oyama and R.M. Yunus, *Curr. Appl Phys*., 10 (2013)1071.
22. M. Deraman, *J. Phys D: Appl. Phys.*, 27 (1994) 1060.
23. Awitdrus, M. Deraman, I.A. Talib, R. Omar, M.H. Jumali, E. Taer and M.M. Saman, *Sains Malaysiana*, 39 (2010) 83.
24. A.R. Coutinho, J.D. Rocha and C.A. Luengo, *Fuel Process. Technol*., 67 (2000) 93.
25. M. Deraman, S.K.M. Saat, M.M. Ishak, Awitdrus, E. Taer, I.A. Talib, R. Omar and M.H. Jumali, *AIP Proceeding*, 1284 (2010) 179.
26. D. Qu, *J. Power Sources*, 109 (2002) 403.
27. Ch. Emmenegger, Ph. Mauron, P. Sudan, P. Wenger, V. Herman, R. Gallay and A. Zuttel, *J. Power Sources*, 124 (2003) 321.
28. M. Khalfaoui, S. Knani, M.A. Hachicha and A. Ben Lamine, *J. Colloid Interface Sci*., 263 (2003) 350.
29. E. Taer, M. Deraman, I.A. Talib, S.A. Hashmi and A.A. Umar, *Electrochim. Acta*, 56 (2011) 10217.
30. F-C. Wu, R-L. Tseng, C-C. Hu, C-C. Wang, *J. Power Sources*, 159 (2006) 1532.
31. W.C. Chen, T.C. Wen and H. Teng, *Electrochim. Acta*, 48 (2003) 641.
32. F. Rafik, H. Guolous, R. Gallay, A. Crausaz and A. Berthon, *J. Power Source*, 165 (2007) 928.
33. Y.R. Nian and H. Teng, *J. Electroanal. Chem.*, 540 (2003) 119.
34. J. Gamby, P.L. Taberna, P. Simon, J.F. Fauvarque and M. Chesneau, *J. Power Sources*, 101 (2001) 109.
35. A. Garcia-Gomez, P. Miles, T.A. Centeno and J.M. Rojo, *Electrochim. Acta*, 55 (2010) 8539.
36. T. Thomberg, A. Janes and E. Lust, *Electrochim. Acta*, 55 (2010) 3138.
37. A.I. Inamdar, Y.S. Kim, S.M. Pawar, J.H. Kim, H. Im, H. Kim, *J. Power Sources*, 196 (2011) 2393.

38. J. Yan, T. Wei, B. Shao, Z. Fan, W. Qian, M. Zhang, F. Wei, *Carbon*, 48 (2010) 487.
39. H. Yu, J. Wu, L. Fan, K. Xu, X. Zhong, Y. Lin and J. Lin, *Electrochim. Acta*, 56 (2011) 6881.
40. K.M. Kim, J.W. Hur, S. I. Jung and A.S. Kang, *Electrochim. Acta*, 50 (2004) 863.
41. M. Olivares-Marin, J.A. Fernandez, M.J. Lazaro, C. Fernandez-Gonzalez, A. Macias-Garcia, V. Gomez-Serrano, F. Stoeckli and T.A. Centeno, *Mater. Chem. Phys.*, 114 (2009) 323.